Large-Scale Magnetic Microcalorimeter Arrays for the Lynx X-Ray Microcalorimeter

Large-Scale Magnetic Microcalorimeter Arrays for the Lynx X-Ray Microcalorimeter

Large-scale magnetic micro-calorimeter arrays for the Lynx X-ray Microcalorimeter

Archana M. Devasia • Simon R. Bandler • Kevin Ryu • Thomas R. Stevenson • Wonsik Yoon

NASA Goddard Space Flight Center, Greenbelt MD 20771, USA
Lincoln Laboratory, Massachusetts Institute of Technology, Lexington MA 02420, USA
Science Systems and Applications Inc., Lanham MD 20706, USA

Abstract The Lynx X-ray Microcalorimeter (LXM) is an imaging spectrometer consisting of an array of greater than 100,000 pixels. Magnetic micro-calorimeter (MMC) technology is a leading contender for detectors for the LXM. In this work, we detail the design of a full-size LXM MMC array fabricated using superconducting, multi-layer, buried wiring, with all pixels wired out on a full-size support wafer. We adopt a scheme that facilitates mixing and matching deep UV (DUV) and i-line (365 nm) steppers to stitch the high feature resolution detector array to the large field fanout wiring. To realize the Main Array of the microcalorimeter we also employ a sandwich geometry. In this type of pixel, a superconducting ground plane placed above a paramagnetic sensor forces most of the magnetic flux to remain inside the sensor. This device aims to improve the coupling of the sensor to the pick-up coil, and thus enhance the energy resolution. Additionally, we introduce the integration of superconducting flux transformers to optimize the performance of the Ultra High Resolution Array. The wiring to each pixel terminates on bump bond pads, which allow future 2D microwave SQUID based multiplexer chips to be indium bump bonded over the buried wiring. We present fabrication results and preliminary room temperature electrical measurements.

Keywords microcalorimeter • superconducting wiring • arrays • Hydra

1 Introduction

The Lynx X-ray Microcalorimeter (LXM) is a broadband, energy-dispersive, high spectral and spatial resolution, imaging spectrometer focal plane instrument [1]. It comprises of over 100,000 pixels arranged into three separate sensor arrays, each designed to meet science requirements of the

Lynx mission concept [2]. The Main Array is designed to provide better than 3 eV energy resolution over the 0.2–7 keV band, and imaging with 1-arcsecond pixels over a 5 arcminutes × 5 arcminutes field of view (FOV), driven equally by requirements of the signal to noise ratio, galaxy cluster, and interstellar medium observations. The Enhanced Main Array (EMA) spans the energy range of 0.2–7 keV with 0.5- arcsecond pixels over a 1 arcminute × 1 arcminute FOV, providing an energy resolution of 2 eV. It will be used for finer spectroscopic-imaging required to characterize the effects of active galactic nucleus (AGN) feedback on the interstellar medium of host galaxies and to measure the physical state of gas near the supermassive black hole sphere of influence. The Ultra High Resolution (UHR) subarray covers the 0.2–0.75 keV band with 1-arcsecond pixels over a 1 arcminute × 1 arcminute FOV, providing 0.3 eV energy resolution required for studies of supernovae-driven galaxy winds and density diagnostics in AGN outflows.

The LXM X-ray detectors, operating at 40 mK, precisely determine incident photon energies by measuring the temperature rise from the heat they deposit. Magnetic Micro-Calorimeter (MMC) technology, which employs the magnetization of a paramagnetic sensor, to detect temperature changes, is a leading contender for such a detector [3]. MMCs have demonstrated energy resolutions as good as 1.7 eV for 6 keV photons [4].

Two major challenges are associated with the fabrication of very large size arrays. As the array size increases, the stray inductance of the wiring, both between pixels and in the fanout to amplifiers also increases, which can degrade the MMC energy resolution performance. Previously we examined how MMC dimensions can be scaled to maintain signal coupling and energy resolution in large arrays despite the increase in stray inductance [5]. To this end we successfully demonstrated submicron pitch MMC devices with high sensor inductance, good magnetic coupling, and large critical currents [6]. The second challenge involves routing the wiring from all the pixels to the multiplexed readout. To achieve this objective, we utilized a planarized, deep-submicron, superconducting wiring technology developed by MIT-Lincoln Laboratory (MIT-LL) [7, 8]. We successfully fabricated large-size MMC arrays with large scale, low inductance, low crosstalk, high density wiring by using multiple buried layers of Nb interleaved with planarized SiO_2 interlevel dielectric (ILD) [6].

In this work we present the design and fabrication of a full-size LXM prototype MMC array. The design integrates the various features described above to produce a very large format focal plane array of 100,000 pixels. It advances current MIT-LL buried wiring technology to beyond baseline and introduces elements that leverage the multi-layer buried wiring capability.

2 Design

2.1 Detector Array

The full-size LXM MMC prototype is a 100 mm wafer size octagon with a central 22 mm x 22 mm area comprising of the detector array as shown in Fig. 1(Left). It is patterned using a Canon FPA-3000 EX4 DUV stepper with 248 nm exposure wavelength. The Enhanced and UHR sub-arrays are ensconced within a surrounding Main Array (Fig. 1(Center)). The detector array is formed using four buried Nb metal layers. The topmost Nb layer (M4) forms the sensor pick-up coils. A twin-microstrip scheme, with pairs of adjacent signal wires over a common ground plane, is adopted to configure the wiring from each sensor. In the Main Array this wiring is located on the same Nb layer as the sensor pick-up coils. In the sub-arrays, the wiring is patterned on the bottom most Nb layer (M1) and connected through superconducting vias to the pick-up coils as illustrated in Fig. 1(Right). The two intermediate buried Nb layers (M2 and M3) function as superconducting ground planes for the Main Array wiring and the sub-array wiring respectively.

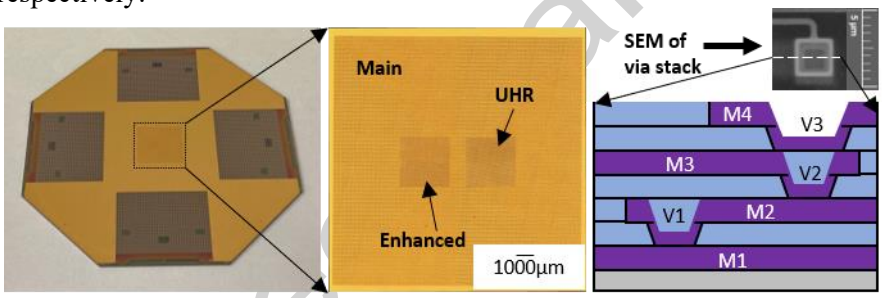

Fig. 1 (*Left)* Fabricated 100 mm wafer size octagonal detector chip. *(Center)* Optical image of detector array located at center of detector chip comprising of a Main Array and EM and UHR sub-arrays. (*Right*) Cartoon showing a cross-sectional view of a stack of vias (V1, V2, V3) connecting the topmost metal layer M4 to the bottom most layer M1. (Color figure online)

The Main Array and the EMA are designed for multi-absorber sensors, where the coupling between a sensor and multiple absorbers is through thermal links of varying dimensions. This 'Hydra' design allows 25 different pixels to be read out from a single sensor. Upon absorption of X-ray photons, each Hydra pixel can be identified by its characteristic pulse shape, which is defined by the unique thermal conductance value of its thermal Hydra link [9]. This thermal multiplexing is implemented by designing each Main array and EMA sensor to have a waffle shaped geometry, which enables absorber stems and Hydra links to be located within the waffle grid. The waffle shape of a Main array sensor is depicted in Fig. 2.

The Main Array is a 60x60 sensor array with two different pixel configurations: a meander coil geometry and a sandwich geometry. In the first type of pixel, a meandering Nb pick-up coil is placed below and thinly insulated from a Au:Er sensor. The persistent current flowing through the coil produces a strongly inhomogeneous magnetic field around the meandering wire of the pick-up loop within the volume of the sensor [2]. Less than half of the magnetic field energy is contained within the sensor volume [10]. To significantly enhance the magnetic coupling efficiency, the sensor can be sandwiched between two superconducting stripes of the pick-up coil, with thin insulation in between, like the device discussed in [10]. A homogenous magnetic field is generated by the current flowing along the two layers, around the sensing material. This field is highly uniform on the Au:Er and does not exist outside it. Because of its homogenous nature, all the field can be close to its optimal value for a given operating temperature. Thus, a sandwich geometry maximizes the volume of Au:Er that has an optimal field on it.

In our detector array, a sandwich device is produced by positioning the Au:Er sensor in between a bottom spiral Nb pick-up coil, and a top superconducting Nb ground plane as shown in Fig. 2. To realize the waffle shaped grid pattern of the sensor, adjacent spiral coils are daisy chained, through a second intermediate Nb layer.

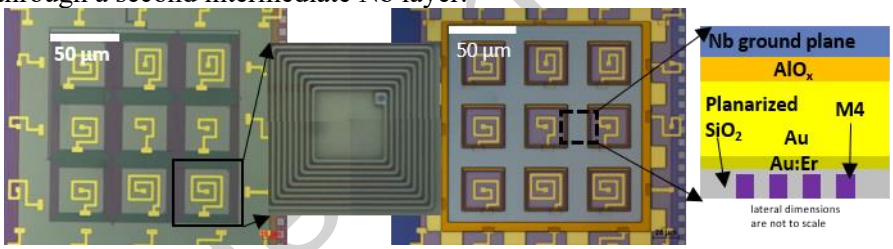

Fig. 2 Sandwich device: *(Left)* Optical image with Au Hydra links and 800 nm pitch rectangular spirals, daisy chained to form a Nb pick-up coil. Inset shows a composite image of four corners of a spiral. *(Center)* Optical image post addition of Au:Er, with a thermalization Au cap to improve diffusivity without significant increase in overall heat capacity, and top Nb ground plane. *(Right)* Cartoon showing cross-sectional view of device. M4 refers to the buried Nb layer forming the spiral pick-up coil. (Color figure online)

The EMA is a 24x24 sensor array with meander coil geometry. It comprises of PdAu Hydra links designed using a multi-arm strategy as shown in Fig. 3(Left). One advantage of using PdAu is that processing conditions, such as annealing history, do not influence its residual resistivity. PdAu being an alloy, its electronic mean free path is short and is set by the composition. It is independent of the crystal grain size, which is affected by annealing history. Main Array Hydra links on the other hand, are fabricated

from Au, because based upon the design value of sheet resistance for these Hydra links (71.1×10^{-3} Ω/sq), and the resistivity of PdAu (28.8×10^{-8} Ω-m), the required PdAu thickness (4.04 μm) would be too high.

The effective measurable energy range of a Hydra detector is limited when the inherent position error of its pixels is non-uniform [11]. The position error is the probability of misidentifying the location of an X-ray hit for a given pixel. The optimal design for each pixel, to ensure uniform positional error, can be achieved by adjusting the thermal conductance values of the Hydra links. In this design we selected a set of thermal conductances in such a way that the distinguishability of the pulse shapes is optimized. A detailed theoretical model of this methodology is under preparation for publication [12].

The multi-arm concept ensures that the thermal links are always longer than they are wide. For wide links which are connected to a narrower absorber stem, the heat flow lines would have to bunch together to enter the narrow stem terminal. Thus, the thermal resistance, and hence the effective number of squares for the link, would be higher than for the case of uniform heat flow. To avoid this, the number of arms (links) is doubled as the width of the link starts approaching the width of the stem.

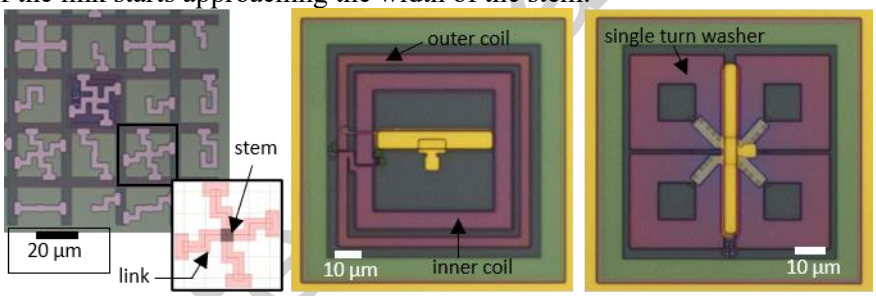

Fig. 3 *(Left)* Optical image of section of waffle shaped EMA sensor meander coil with PdAu Hydra links. Inset shows location of absorber stem. *(Center)* Optical image of UHR pixel with a dual concentric flux transformer structure. Inner and outer coils are covered by a ground plane. (*Right)* Optical image of UHR pixel with a single turn washer. The multi-turn coil lies below the washer and hence is not visible. (Color figure online)

The UHR Array in a 32x32 single-pixel (non-Hydra) sensor array, where in each pixel, a Au thermal link connects the absorber stem to the sensor. This thermal link reduces the thermal signal rise-time, and thus controls the size of the signal-current slew rate, making the readout easier. For each pixel type, the area of the Au:Er is designed to match the sensor heat capacity to the absorber heat capacity. In our previous generation of devices, we eschewed this approach for UHR pixels since a small Au:Er area would have resulted in a meager sensor inductance that is much smaller than the stray

inductance [6]. In this full-size LXM prototype, we stepped up the sensor inductance through the introduction of flux transformers, catalyzed by the ability to use multiple layers of buried wiring. Two different transformer types have been designed with a goal to get good energy coupling efficiency, and the highest output inductance that can be obtained in the given unit cell area, with the number of available buried Nb layers. In the first design, shown in Fig. 3(Center), the input and output coils are concentric and formed on two distinct Nb layers. Both coils are counter wound with twice as many turns in their inner section as their outer section. The sensor meander coil is located at the center of the two concentric coils. The second design, illustrated in Fig. 3(Right), has a multi-turn gradiometric output coil on one Nb layer and a single turn washer on a different Nb layer. The sensor meander coil is nestled between the two halves of the Nb washer. Each transformer design has an output inductance of several nH, which is greater than or comparable to the array wiring stray inductance. Both types of transformers are surrounded by a superconducting streets ground plan that carries the array wiring. The output inductance of the gradiometric design is expected to be greater than that of the dual concentric design by a factor of 5. However, the dual concentric design was expected to be more immune to performance degradation from screening by the ground plane in the streets.

2.2 Fanout

The area outside the central 22 mm x 22 mm region accommodates the fanout wiring from ~5k MMC sensors in the detector array. This is accomplished by using a Canon i-line (365 nm) stepper with a larger 50 mm x 50 mm field, referred to as iW. Covering a 100 mm wafer sized area requires four separate iW fields, as shown in Fig. 4(Left). To reduce fabrication complexity, each quadrant has its own set of reticles and no stitching between iW fields is utilized. Additionally, to prevent fabrication costs from becoming prohibitive, in this first iteration of a full-size LXM prototype, we elected to restrict the number of Nb buried wiring layers in the iW fields to two (M3 and M4 only).

As discussed in section 2.1, the EX4 detector field fanout is on two separate Nb layers (M1 and M4). Prior to transitioning to the iW fields, this multi-level wiring from the sensor array is relocated onto the same Nb layer (M3). The stitching between EX4 and iW fields is accomplished 1 μm inside the edge of the detector field. In the iW fields, the fanout is on one Nb layer (M3) and runs under a superconducting ground plane formed by the second Nb layer (M4) as shown in Fig. 4(Center). The fanout from most pixels terminates on bump bond pads, with a select few connected to wire bond pads. To minimize stray wiring inductance, the fanout to the bump bond pads gets progressively wider as it moves away from the central detector

region and advances towards the octagon edge, producing a 2D array of pads. Future 2D microwave SQUID (mSQUID) based multiplexer (μMUX) chips will be indium bump bonded to these pads, forming an mSQUID array. In its current incarnation, without an mSQUID, a unit cell of the mSQUID array comprises of a pair of pads surrounded by a Nb ground plane (Fig. 4(Right)). The oxide over the ground plane is removed in order to have a clean Nb shield under each microwave resonator for high Q and low two-level system noise. Additionally, the ground plane has a cut-out to avoid screening the SQUID input transformer. Fig. 5(Left) shows a cartoon of future μMUX chips bump bonded to an mSQUID array, one per quadrant.

The iW fields also house superconducting ballast inductors, which are large load inductances that provide a near constant current bias when a persistent current is stored in the circuit. Each octant contains two meandered ballast inductors (each 10.1 μH), one for the Main Array bias circuit and the other for a sub-array circuit. They are fabricated on the same Nb layer as the fanout and fill the space between adjacent mSQUID arrays.

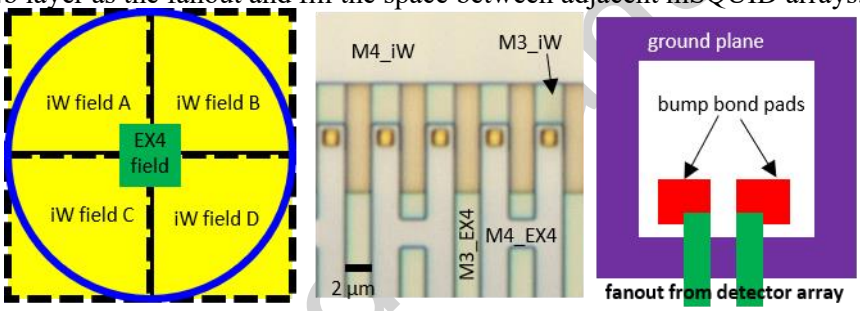

Fig. 4 *(Left)* Location of EX4 and iW fields. *(Center)* Optical image of EX4 to iW transition region. Metal layer M4_EX4 in the EX4 field is relocated to layer M3_iW in the iW field. The superconducting ground plane M3_EX4 in the EX4 field has switched positions with M4_iW in the iW field. *(Right)* Cartoon of mSQUID unit cell showing annular ground plane enclosing pads connected to fanout from a sensor in the detector array. (Color online)

2.3 Fabrication

The buried wiring process is carried out on 200 mm Si wafers at MIT-LL. Details on the fabrication of buried layers are available in [6-8]. Mixing and matching EX4 and iW reticles occurs for the layers that are common between the two fields i.e. the top two Nb layers, and their corresponding ILDs. Patterning and etching these four layers involve, (a) exposing EX4 reticle and etching, (b) exposing iW reticle, for each quadrant, and etching.

One 100 mm detector wafer is cored out of each 200 mm wafer. After coring, processing is continued at NASA GSFC's Detector Development Laboratory. Pads for future indium bumps are formed by nitridization of Mo.

In order to realize the top superconducting Nb (250 nm) ground plane for the sandwich geometry devices, we elected to use a lift-off technique. In this process, Nb is patterned using a Ge hard mask that caps an underlying photoresist lift-off mask. During Nb deposition, the Ge blocks the photoresist from outgassing, and thus prevents the incorporation of C or N_2 [13]. The lift-off method also preserves the integrity of the exposed Nb ground planes of the mSQUID array, which would otherwise have been attacked, had an etch process been employed to pattern the sandwich Nb. This Nb is insulated from the Au:Er through 200 nm thick Al_2O_3, deposited by e-beam evaporation. Details on other layers can be found in [6].

3 Results

A successfully fabricated full-size LXM MMC prototype octagon is illustrated in Fig 1. Optical images of various elements that have been introduced in this generation are shown in Fig. 2-4. In our previous devices, sections of the waffle shaped EMA sensor were vulnerable to direct hits from incoming X-rays due to large gaps between adjacent absorbers in the 5x5 Hydra (Fig. 5(Center). To mitigate the impact of this issue, in this work, the area fill factor for X-rays is increased from 64% to 84.64% (Fig. 5(Right). This is accomplished by reducing the absorber gap size between pixels with an optimized ion milling etch for the absorbers.

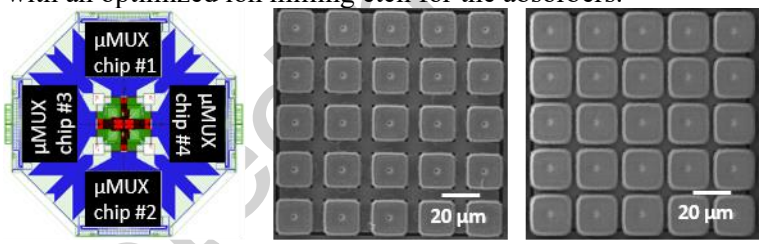

Fig. 5 *(Left)* Cartoon of MMC prototype octagon showing locations of future µMUX chips. *(Center)* SEM image of previous generation of EMA composite Hydra absorber with large gaps between pixels. *(Right)* SEM image of current generation of EMA Hydra absorber with narrower gaps between adjacent pixel absorbers. (Color online)

Room temperature electrical measurements are carried out to test continuity between EX4 and iW fields, and isolation between the large Main and sub-array ballast inductors. Results are tabulated below (Table 1)

Test and location	Measured value (Ω		Expected value (Ω
	W#1	W#2	
Main Array pixel, quadrant A	106.3 K	122.6 K	118 K
EMA pixel, quadrant C	69.2 K	72.9 K	78.9 K
UHR Array pixel, quadrant B	57.8 K	58.2 K	63 K

Main Array ballast inductor, quadrant D	24.3 M	24.1 M	26.5 M
Isolation between Main and sub-array ballast inductors, quadrant C	73.4 M	77.9 M	Open

Table 1 Room temperature resistance measurements on two different wafers

In the previous generation, measurements carried out on wiring test structures have indicated a yield of 100%. Although not representative of cold working devices, the room temperature screening described in Table 1 implies that we have pushed the buried wiring process to an extent where defects in the process are now detectable. Detector performance will be measured on these devices in the near future.

4 Conclusion

We have successfully fabricated a full-size LXM MMC prototype. Our approach uses the synergy between a high-resolution stepper and a large field stepper to realize fine pitch MMC devices and route the wiring from 100,000 pixels to the multiplexed readout. We have integrated 'sandwich' devices and superconducting flux transformers into our design, which will allow us to explore further enhancements in performance.

Acknowledgements Work performed at MIT Lincoln Laboratory is based on work supported by NASA's ROSES 2017: Astrophysics Research and Analysis program under Air Force Contract No. FA8702-15-D-0001.

Data Availability The datasets generated during and/or analysed during the current study are available from the corresponding author on reasonable request.

References

1. A. Vikhlinn, F. Ozel, J. Gaskin, Lynx Concept Study Report 2020. https://wwwastro.msfc.nasa.gov/lynx/docs/LynxConceptStudy.pdf
2. S.R. Bandler, J.A. Chervenak, A.M. Devasia et al., J. Astron. Telesc. Instrum. Syst **5(2)**, 021017 (2019), DOI: 10.1117/1.JATIS.5.2.021017
3. A. Fleischman, C. Enss, G.M. Seidel, in Cryogenic Particle Detection, Topics in Applied Physics, ed. By C. Enss, (Springer, Berlin, Heidelberg, 2005), p. 151
4. J.-P. Porst, S.R. Bandler, J.S. Adams et al., J. Low Temp. Phys. **175**, 617 (2014), DOI: 10.1007/s10909-013-1019-y
5. T.R. Stevenson, M.A. Balvin, S.R. Bandler et al., J. Low Temp. Phys. **193**, 668 (2018), DOI: 10.1007/s10909-018-1956-6

6. A.M. Devasia, M.A. Balvin, S.R. Bandler et al., IEEE Trans. Appl. Supercond. **29**, (2019), DOI: 10.1109/TASC.2019.2902530
7. S.K. Tolpygo, V. Bolkhovsky, T.J. Weir et al., IEEE Trans. Appl. Supercond. **25**, (2015), DOI: 10.1109/TASC.2014.2369213
8. S.K. Tolpygo, V. Bolkhovsky, T.J. Weir et al., IEEE Trans. Appl. Supercond. **26**, (2016), DOI: 10.1109/TASC.2016.2519388
9. S.J. Smith, S.R. Bandler, R.P. Brekosky et al., IEEE Trans. Appl. Supercond. **19**, (2009), DOI: 10.1109/TASC.2009.2019557
10. C. Pies, S. Schafer, S. Heuser et al., J Low Temp. Phys. **167**, 269 (2012), DOI: 10.1007/s10909-012-0557-z
11. W. Yoon, M.A. Balvin, S.R. Bandler et al., J. Low Temp. Phys. **199,** 916 (2020), DOI: 10.1007/s10909-019-02311-6
12. T.R. Stevenson, W. Yoon, *Optimization of thermal links in multipixel sensors for X-ray microcalorimeters*, in preparation for publication.
13. A. Brown, A. Patel, High Precision Metal Film Liftoff Technique, U.S. Patent 9,076,658 B1, filed September 25, 2014, and issued July 7, 2015.